mTORC2 Activity Disrupts Lysosome Acidification in Systemic Lupus Erythematosus by Impairing Caspase-1 Cleavage of Rab39a

Andrew J. Monteith,* Heather A. Vincent,* SunAh Kang,* Patrick Li,* Tauris M. Claiborne,* Zenon Rajfur,[†,‡] Ken Jacobson,[†] Nathaniel J. Moorman,* and Barbara J. Vilen*

Lysosomes maintain immune homeostasis through the degradation of phagocytosed apoptotic debris; however, the signaling events regulating lysosomal maturation remain undefined. In this study, we show that lysosome acidification, key to the maturation process, relies on mTOR complex 2 (mTORC2), activation of caspase-1, and cleavage of Rab39a. Mechanistically, the localization of cofilin to the phagosome recruits caspase-11, which results in the localized activation of caspase-1. Caspase-1 subsequently cleaves Rab39a on the phagosomal membrane, promoting lysosome acidification. Although caspase-1 is critical for lysosome acidification, its activation is independent of inflammasomes and cell death mediated by apoptosis-associated speck-like protein containing a caspase recruitment domain, revealing a role beyond pyroptosis. In lupus-prone murine macrophages, chronic mTORC2 activity decouples the signaling pathway, leaving Rab39a intact. As a result, the lysosome does not acidify, and degradation is impaired, thereby heightening the burden of immune complexes that activate FcγRI and sustain mTORC2 activity. This feedforward loop promotes chronic immune activation, leading to multiple lupus-associated pathologies. In summary, these findings identify the key molecules in a previously unappreciated signaling pathway that promote lysosome acidification. It also shows that this pathway is disrupted in systemic lupus erythematosus. ***The Journal of Immunology*****, 2018, 201: 371–382.**

Extracellular cargo can be internalized through endocytosis, phagocytosis, or LC3A-associated phagocytosis (LAP). Following internalization, the exchange of small Rab GTPases on vesicular membranes dictates trafficking (1), whereas ESCRT proteins associated with ubiquitinated proteins/receptors on vesicular membranes promote lysosomal degradation (2). Following the fusion of phagosomes with lysosomes, recruitment of LAMP proteins stabilizes the membrane (3), and assembly of the vacuolar H^+-ATPase (V-ATPase) facilitates acidification (4). Although phagosomal maturation requires the association of numerous proteins, fundamentally it is a two-step process. First, assembly of the NADPH oxidase on the phagosomal membrane initiates the oxidative burst that transfers electrons to molecular oxygen-producing reactive oxygen species (5). Second, termination of the oxidative burst and assembly of the V-ATPase acidifies the phagosome, activating hydrolytic enzymes that degrade internalized cargo (6).

Proteins not directly involved in vesicular trafficking also influence lysosomal degradation. During infection, microbes manipulate ARP2/3 and cofilin, thereby dysregulating the actin cytoskeleton, resulting in lysosome collapse and altered phagosome–lysosome fusion (7, 8). Further, caspase-1 and caspase-11 are critical for lysosome acidification following phagocytosis of *Staphylococcus aureus* and *Legionella pneumophila* (9, 10). Also, mammalian target of rapamycin (mTOR) associates with the lysosome and senses amino acid levels through an "inside-out" mechanism (11). How the actin cytoskeleton, pyroptotic caspases, and mTOR influence lysosome function remains unclear.

Despite an incomplete understanding of the events controlling lysosome function, many diseases are associated with lysosomal defects, including cardiovascular disease, cancer, and neurodegeneration (12). In addition, we recently reported that lysosome maturation is defective in systemic lupus erythematosus (SLE), in which macrophages (Mφs) fail to degrade immune complexes (ICs) formed by IgG binding to apoptotic blebs (IgG-ICs) (13). Coincident with elevated FcγRI signal transduction (14), intact IgG-ICs are recycled to the cell membrane bound to FcγRs where they accumulate (13). Accumulation of nuclear Ags on the surface of the immune cells occurs prior to SLE-associated pathologies in MRL/*lpr* mice (14), and impaired degradation of IgG-ICs heightens BAFF, IFN-α, autoantibodies, cell death, B cell expansion, and lupus nephritis (13–15). Additionally, accumulation

*Department of Microbiology and Immunology, University of North Carolina at Chapel Hill, Chapel Hill, NC 27599; [†]Department of Cell Biology and Physiology, University of North Carolina at Chapel Hill, Chapel Hill, NC 27599; and [‡]Department of Physics, Astronomy, and Applied Computer Science, Institute of Physics, Jagiellonian University, 31-007 Krakow, Poland

ORCIDs: 0000-0002-6327-184X (S.K.); 0000-0003-0014-0022 (B.J.V.).

Received for publication December 12, 2017. Accepted for publication May 8, 2018.

This work was supported by National Institutes of Health (NIH) Grants R21AI105613 and R21AR064951, the Rosemarie K. Witter Foundation, and the Lupus Research Alliance. A.J.M. was supported by NIH Grant 5T32AI07273. The Flow Cytometry Core and the Microscopy Services Laboratory were supported by NIH Grant P30 CA016086.

Address correspondence and reprint requests to Dr. Barbara J. Vilen, University of North Carolina at Chapel Hill, 6110 Marsico Hall, CB 7290, 125 Mason Farm Road, Chapel Hill, NC 27599-7290. E-mail address: barb_vilen@med.unc.edu

The online version of this article contains supplemental material.

Abbreviations used in this article: AMPK, 5′ AMP-activated protein kinase; ASC, apoptosis-associated speck-like protein containing a caspase recruitment domain; B6, C57BL/6J; BMMφ, bone marrow Mφ; Casp1$^{-/-}$, B6.*caspase-1*$^{-/-}$; Casp 11$^{-/-}$, B6.*caspase-11*$^{-/-}$; CRP, C-reactive protein; IC, immune complex; IgG-IC, IC formed by IgG binding to apoptotic bleb; JasP, Jasplakinolide; LAP, LC3A-associated phagocytosis; LCM, L cell medium; LIMK, Lim kinase; Mφ, macrophage; MFI, median fluorescence intensity; mTOR, mammalian target of rapamycin; mTORC1, complex 1; mTORC2, mTOR complex 2; Rab39a[CT], Rab39a C-terminal; Rab39a[NT], Rab39a N-terminal; rpS6, ribosomal protein S6; SLE, systemic lupus erythematosus; V-ATPase, vacuolar H^+-ATPase; WC-IC, apoptotic cell opsonized by IgG.

of IgG-ICs is found in other murine models of SLE, including NZM2410 (13, 14). This supports a model in which lysosome defects promote inflammation during SLE pathogenesis. Therefore, impaired lysosomal maturation in lupus-prone Mφs provides a disease-relevant model to identify signaling events associated with lysosome maturation.

This study reveals that the cleavage of Rab39a by locally activated caspase-1 occurs on the surface of phagocytic vesicles and is necessary for lysosome acidification. This process requires cofilin association with the actin that surrounds the vesicle and recruits caspase-11, which locally activates caspase-1. In turn, caspase-1 cleaves Rab39a to promote lysosome acidification. In lupus-prone Mφs, this cascade is defective because chronically active mTOR complex 2 (mTORC2) heightens cofilin phosphorylation, thereby disrupting its binding to actin, a critical early step in the pathway to acidification. As a consequence, caspase-11 is not recruited to the vesicle, the localized activation of caspase-1 is reduced, Rab39a is not cleaved, and the lysosome does not fully acidify. By using a disease model harboring defects in lysosome maturation, we define the key molecules in a previously unappreciated signaling cascade that are necessary for lysosome acidification.

Materials and Methods

Mice

C57BL/6J (B6) and MRL/MpJ-*Tnfrs6*^{lpr}/J (MRL.Fas^{lpr}; MRL/*lpr*; JAX mice stock no. 000485) colonies were maintained in an accredited animal facility. The B6.*caspase-1*$^{-/-}$ (Casp1$^{-/-}$) (16), B6.*caspase-1*$^{-/-}$*caspase-11*$^{-/-}$ (Casp1$^{-/-}$Casp11$^{-/-}$) (17), and B6.*pycard*$^{-/-}$ (18) mice were obtained from Dr. E. Miao. The B6.*caspase-1*$^{-/-}$*caspase-11*^{tg} (16) mice were obtained from Dr. J. Ting. FcγRI$^{-/-}$MRL/*lpr* and AID$^{-/-}$MRL/*lpr* mice were previously described (14).

Reagents

Abs specific for CD11b were from BD Biosciences; ribosomal protein S6 (rpS6), p-rpS6, p-Akt^{S473}, p-Akt^{T308}, Akt, 5′ AMP-activated protein kinase (AMPK), p-AMPK, tubulin, mTOR, LC3A, p-cofilin, cofilin, caspase-11, and FLAG were from Cell Signaling Technology; caspase-1 was from Genentech; HA was from Abcam; CD40, CD80, and anti-rabbit IgG were from BioLegend Pharmaceuticals; anti-goat and -rabbit (Alexa 647) IgG were from Molecular Probes; Concanamycin A was from Sigma-Aldrich; LimKi 3 and Jasplakinolide (JasP) were from EMD Calbiochem; Torin1 was from Tocris Bioscience; rapamycin was from Cell Signaling Technology; IRDye680- and IRDy800-conjugated Abs (anti-rabbit, anti-mouse) were from LI-COR Biosciences; phalloidin and LysoSensor Yellow/Blue dextran were from Thermo Fisher; streptavidin (PE) was from Jackson ImmunoResearch; and FAM-FLICA Caspase-1 Assay Kit was from ImmunoChemistry Technologies. Abs specific to nucleosome (PL2-3), Smith (2.12.3), and CD16/32 (2.4G2) and L cell media (LCM) for bone marrow Mφ (BMMφ) differentiation were generated as previously described (13).

BMMφ cultures

BMMφs from 6- to 10-wk-old mice (prior to the onset of disease) were derived as previously described (13), with the exception that cells derived for 5 d (rather than 7) were grown in 15% LCM (rather than 10%) to accelerate differentiation. Increasing the concentration of M-CSF increased the rate of Mφ differentiation while maintaining comparable levels of CD11b, CD40, and CD80. BMMφs cultured in 15% LCM for 5 d or 10% LCM for 7 d were 90–98% CD11b^{+}, I-A^{lo}, and B7.2^{lo}.

Formation of ICs

Apoptotic cells from irradiated thymocytes were pelleted (5 min 350 × *g*). To form apoptotic cells opsonized by IgG (WC-ICs), the pellets were resuspended in 2.5 ml of R10 (RPMI 1640 with 10% FBS). To form IgG-ICs, the supernatant-containing apoptotic blebs were recovered (13). Whole apoptotic cells (1 ml of resuspended pellet) or apoptotic blebs (1 ml of supernatant) were cultured with IgG (6.67 μg) at 4˚C for 75 min to form WC-ICs or IgG-ICs, respectively.

Fluorescent microscopy

BMMφs were cultured with IgG-ICs (Alexa 647) in R10 media for 2 h at 37˚C, fixed with 2% paraformaldehyde at 4˚C for 15 min, blocked in 2.4G2 (FcγR block) for 30 min at 4˚C in FACS media (PBS with 2% FBS, 0.02% NaN_3), washed, and then stained with primary and secondary Abs, or nuclear-stained with Hoechst 33342 (1μg/ml), in permeabilization buffer (PBS with 0.05% saponin and 0.5% BSA) for 30 min at 4˚C. Mφs attached to glass-bottom dishes were imaged in FACS media, whereas unattached Mφs were resuspended in FluorSave. All confocal microscopy used a Zeiss 710 confocal microscope with a 63 × 1.4 numerical aperture (oil) Plan Apo lens and Zeiss Zen Software. Images were analyzed using ImageJ. Colocalization was measured by calculating the Mander's overlap coefficient (colocalized pixels/total fluorescent pixels).

Cellular motility assays

BMMφs were plated onto glass coverslips for 48 h. To quantify membrane ruffling, a kymograph (perpendicular to the cell membrane) was generated for each cell. The persistence and average velocity for membrane extension and retraction were measured. For migration, BMMφs were plated onto fibronectin-coated glass coverslips for 24 h. The percentage of migrating cells was quantified per field of view over a 2-h time course. Average velocity and persistence of migration were quantified for each migrating cell.

Flow cytometry

BMMφs were warmed (37˚C, 5% CO_2) for 2 h prior to the addition of 40 μl of IgG-ICs in R10 media (as above). To quantify pH in a cell that had not acidified, concanamycin A (20 ng/ml) was introduced to one sample from each treatment and/or background 1 h prior to addition of IgG-ICs and then left on the cells throughout the experiment. IgG-ICs and LysoSensor (2 mg/ml) were cocultured with the BMMφs for 30 min, cells were pelleted, and media was replaced with fresh rhodamine-free R10 media. Cells were incubated for the indicated time points and then analyzed by flow cytometry. The dye was excited with a UV laser (355 nm). Relative pH was quantified by calculating the ratio of the median fluorescence intensity (MFI) from the emission channels (450/20, 585/42 nm) and normalized to the concanamycin A–treated control. Absolute pH was estimated from the ratio of the emission channels by establishing a calibration curve (13). In this study, identical samples were analyzed by flow cytometry and confocal microscopy against solutions of known pH. A ratio of 1 corresponded to a basal pH of 6.7, ratios of 0.6–0.7 corresponded to a pH of 4, and ratios of 0.85–0.95 corresponded to a pH of 5.5–6.

To analyze surface and intracellular proteins in BMMφs, harvested cells were resuspended in FACS media and stained (as above), and the MFI of the indicated proteins was determined by flow cytometry and normalized to an isotype control. All flow cytometry was conducted using an 18-color BD LSR II flow cytometer, and data were acquired using BD FACSDiva 8.0.1 software.

Immunoprecipitation and immunoblot

Cells were lysed in buffer containing 1% CHAPS, 150 mM NaCl, 10 mM Tris (pH 7.5), 2 mM sodium orthovanadate, 1 mM PMSF, 0.4 mM EDTA, 10 mM NaF, and 1 μg/ml (each) aprotinin, leupeptin, and α-1–antitrypsin and were then held on ice for 10 min followed by the removal of particulate material by centrifugation at 12,000 × *g* for 10 min at 4˚C. Immunoprecipitating Abs were conjugated to cyanogen bromide–activated Sepharose 4B per the manufacturer's instructions (Amersham Pharmacia Biotech). Approximately 2 μg of precipitating Ab was incubated with 1.5 × 10^6 cell equivalents of cleared lysate for 2 h at 4˚C. Immunoprecipitates were washed, resuspended in reducing SDS-PAGE sample buffer, and then fractionated by 10 or 15% SDS-PAGE. Separated proteins were transferred to Immobilon-FL Membranes, blocked in LI-COR Blocking Buffer, and then incubated with the various immunoblotting Abs and fluorophore-conjugated secondary Abs. Immunoreactive proteins were detected using a LI-COR Odyssey Infrared Imaging System with Odyssey 3.0 software.

Generation of Rab39a plasmids

Wild type Rab39a– and Rab39aD148A–containing, N-terminal HA and C-terminal FLAG epitopes (primers: Rab39a forward and Rab39a reverse), and the Rab39a N-terminal (Rab39a[NT]) (primers: Rab39a forward and Rab39a[NT] reverse) and Rab39a C-terminal (Rab39a[CT]) (primers: Rab39a[CT] forward and Rab39a reverse) constructs were amplified from *pMXsIG mRAb39a wt* plasmid and *pMXsIG mRab39a mut* plasmid. The amplified products were cloned into pCDNA3.1/V5-His digested with BamHI and XhoI using Gibson (New England BioLabs) cloning, and sequences were confirmed.

The PCR primers used to generate Rab39a include: Rab39a forward: 5′-GGATCTAGCTAGTTAATTAAGGATCCGCCATGTACCCATACGATG-TTCCAGATTACGCTATGGAGACTATTTGGATCTATC-3′ and Rab39a reverse: 5′-GGCGCGCCGGCCCTCGAGTCACTTGTCGTCATCG-TCTTTGTAGTCACAGAAGCACTCTTT-3′. The PCR primers used to generate the N- and C-terminal fragments of Rab39a include: Rab39a CT forward: 5′-GGATCTAGCTAGTTAATTAAGGATCCGCCATGTGTGG-AATGAAGTACATAGA-3′ and Rab39a NT reverse: 5′- GGCGCGCCG-GCCCTCGAGTCATTAGTCTGTTGACAGTCTTTCAGC-3′.

Retroviral transduction

Platinum-E Retroviral Packaging Cells were used to create retroviral particles containing Rab39a constructs per the manufacturer's instructions (Cell Biolabs, San Diego, CA). During derivation, Mφs were transduced on day 2 using 200 μl of BMMφ media (15% LCM) + polybrene (5 μg/ml) in a 24-well low-cluster plate (37°C, 5% CO_2). After 6 h, 1 ml of BMMφ media (15% LCM) was added to each well, and the cells were cultured for another 3 d. By day 5, BMMφs were fully derived, and transduced cells (10–14% of $CD11b^+$ cells) predictably expressed HA and FLAG only when the corresponding N- or C-terminal fragment was present.

Statistics

For microscopy-based experiments, representative images are provided along with quantification of all cells imaged. Error bars represent variation between cells (mean). Error bars in all other assays represent the variation between mice (mean). All p values were calculated using an unpaired t test, one-way ANOVA (Newman–Keuls posttest), or two-way ANOVA when applicable. Significance is indicated on the graphs as follows: $p > 0.05$ (not significant), $*p \leq 0.05$, $**p \leq 0.01$, and $***p \leq 0.001$.

Results

Chronic mTORC2 activity prevents lysosome acidification

Lupus-prone MRL/MpJ-*Tnfrs6*^{lpr}/J (MRL.Fas^{lpr}; MRL/*lpr*) mice develop spontaneous autoimmunity characterized by the production of autoreactive Abs and glomerulonephritis (19). Although the *Fas*^{lpr} deficiency accelerates autoimmunity, the MRL background confers the accumulation of surface-bound IgG-ICs, in part, bound to FcγRI (14, 15). To assess whether FcγRI signaling is chronically activated in MRL/*lpr* Mφs, we quantified phosphorylated signaling effectors downstream of FcγRI (20). Phosphorylation of rpS6 reflects the activity of mTORC1 (21). Prior to stimulation with IgG-ICs, BMMφs derived from lupus-prone MRL/*lpr* mice exhibited a 5.3-fold increase in p-rpS6 compared with BMMφs from B6 mice (Fig. 1A, 1B). Following stimulation with IgG-ICs, the levels of p-rpS6 in MRL/*lpr* Mφs remained 4.8-fold higher than B6, indicating chronically active mTORC1. mTORC2 and PI3K activity are upstream of p-Akt^{S473} and p-Akt^{T308}, respectively (22, 23). Unstimulated MRL/*lpr* Mφs exhibited 3.4- and 3.1-fold increases in basal levels of these effectors compared with B6 cells. Following stimulation with IgG-ICs, MRL/*lpr* Mφs retained a 2.3- and 2.5-fold increase in p-Akt^{S473} and p-Akt^{T308}, suggesting that mTORC2 and PI3K are chronically active in MRL/*lpr* Mφs (Fig. 1A, 1B, Supplemental Fig. 1A, 1B).

To assess whether the activation of the PI3K/Akt/mTOR pathway in MRL/*lpr* Mφs derived from FcγRI, we assessed the levels of these effectors in BMMφs from FcγRI$^{-/-}$MRL/*lpr* mice. We found that BMMφs from FcγRI$^{-/-}$MRL/*lpr* mice exhibited levels of p-Akt$^{S473/T308}$ that were comparable to B6 (Fig. 1A, 1B). This implicates FcγRI signal transduction in heightened activation of mTORC2 and PI3K in MRL/*lpr* mice. In contrast, the increased mTORC1 activity (as measured by rpS6 phosphorylation) was reduced only 2.4-fold in FcγRI$^{-/-}$MRL/*lpr* Mφs compared with MRL/*lpr* (Fig. 1A, 1B), suggesting receptors other than FcγRI are involved in mTORC1 activation, possibly through a MEK/ERK-dependent process (24). Elevated p-rpS6 levels were not dependent on AMPK because p-AMPK and total AMPK levels were not different in MRL/*lpr* BMMφs (Supplemental Fig. 1A, 1B). Consistent with ex vivo Mφs (14), these data indicate that FcγRI signaling underlies chronic PI3K and mTORC2 activity and contributes to mTORC1 activity.

The subcellular location of mTOR is critical for balancing cell growth and nutrient availability. For example, localization of mTOR at the cell membrane is important for insulin signaling and cytoskeletal rearrangements (25, 26), whereas localization to lysosomal membranes is important in amino acid sensing (11). In MRL/*lpr* Mφs, there was 3.5-fold more mTOR localized to the cell membrane compared with B6 (Fig. 1C, 1D). This difference was not due to heightened mTOR expression (Fig. 1E). Rather, it reflects mTOR activity because inhibiting mTORC1 and mTORC2 (mTORC1/C2) with Torin1 (27) reduced mTOR localization to the cell membrane (Fig. 1C, 1D). In addition, staining for RICTOR (mTORC2) and RAPTOR (mTORC1) revealed comparable localization at the membrane in B6 and MRL/*lpr* Mφs (Supplemental Fig. 1C–E). Treatment with Torin1 did not displace RICTOR or RAPTOR from the membrane of either B6 or MRL/*lpr* BMMφs, suggesting that localization of RICTOR and RAPTOR at the membrane is independent of activity. Thus, the chronic localization of active mTOR at the cell membrane likely consists of both RICTOR and RAPTOR complexes localized to PIP_3 (25, 26).

To assess whether chronic mislocalization of mTOR at the cell membrane disrupts lysosome acidification, we measured the pH of the vesicles containing IgG-ICs. For these experiments, we used LysoSensor Yellow/Blue dextran. This dye is internalized with IgG-ICs during phagocytosis, and the conjugation to dextran restricts the dye to the phagosome. This allows for specific quantification of phagosome acidification during maturation and fusion with the lysosome. Using single-cell microscopy with standards, we previously demonstrated that B6 Mφs treated with a V-ATPase inhibitor exhibit a basal pH = 6.7 (13). Following phagocytosis of IgG-ICs, B6 Mφs acidify to a pH of 4 (13). For ratiometric flow cytometry, we normalized the unacidified phagosome (pH = 6.7) to 1, with a pH of 4 corresponding to a relative pH of 0.6–0.7 (13). In contrast, MRL/*lpr* Mφs failed to sustain a pH below 5.5 corresponding to a relative pH ranging from 0.85–0.95 (13). Consistent with our previous study, stimulating B6 Mφs with IgG-ICs induced a 22% decrease in vesicular pH (pH ≤ 4.5) within 30 min (Fig. 2A, gating scheme in Supplemental Fig. 1F). In contrast, MRL/*lpr* Mφs showed an 8% decrease in pH (pH ≥ 5.5), indicating lysosome acidification is impaired. The inability of MRL/*lpr* Mφs to acidify lysosomes is the result of mTOR activity because treatment with Torin1 restored acidification to levels comparable to B6 (Fig. 2A).

Previously, we reported that diminished lysosome acidification promotes the recycling of IgG-ICs because hydrolase activity is reduced at a suboptimal pH (13). Coinciding with restored lysosome acidification, Torin1 treatment prevented MRL/*lpr* Mφs from recycling IgG-ICs to the cell membrane (Fig. 2B). In B6 Mφs, Torin1 treatment also reduced the basal level of IgG-IC recycling, suggesting that inhibition of mTORC1/C2 broadly enhances the degradative capacity of the lysosome. To decipher whether mTORC1 and/or mTORC2 were important in lysosome acidification, we compared treatment with Torin1 to rapamycin; a potent inhibitor of mTORC1 (28). In MRL/*lpr* Mφs, treatment with rapamycin inhibited mTORC1, whereas treatment with Torin1 inhibited the activity of mTORC1/C2 (Supplemental Fig. 1G). Unlike Torin1, rapamycin treatment was not sufficient in restoring lysosome acidification in MRL/*lpr* Mφs (Fig. 2A). These data suggest a specific role for mTORC2 in lysosome acidification. Because autophagy is inhibited by mTORC1 activity (29), and rapamycin (mTORC1 inhibitor) did not restore acidification (Fig. 2A), it is unlikely that autophagy is involved in degrading

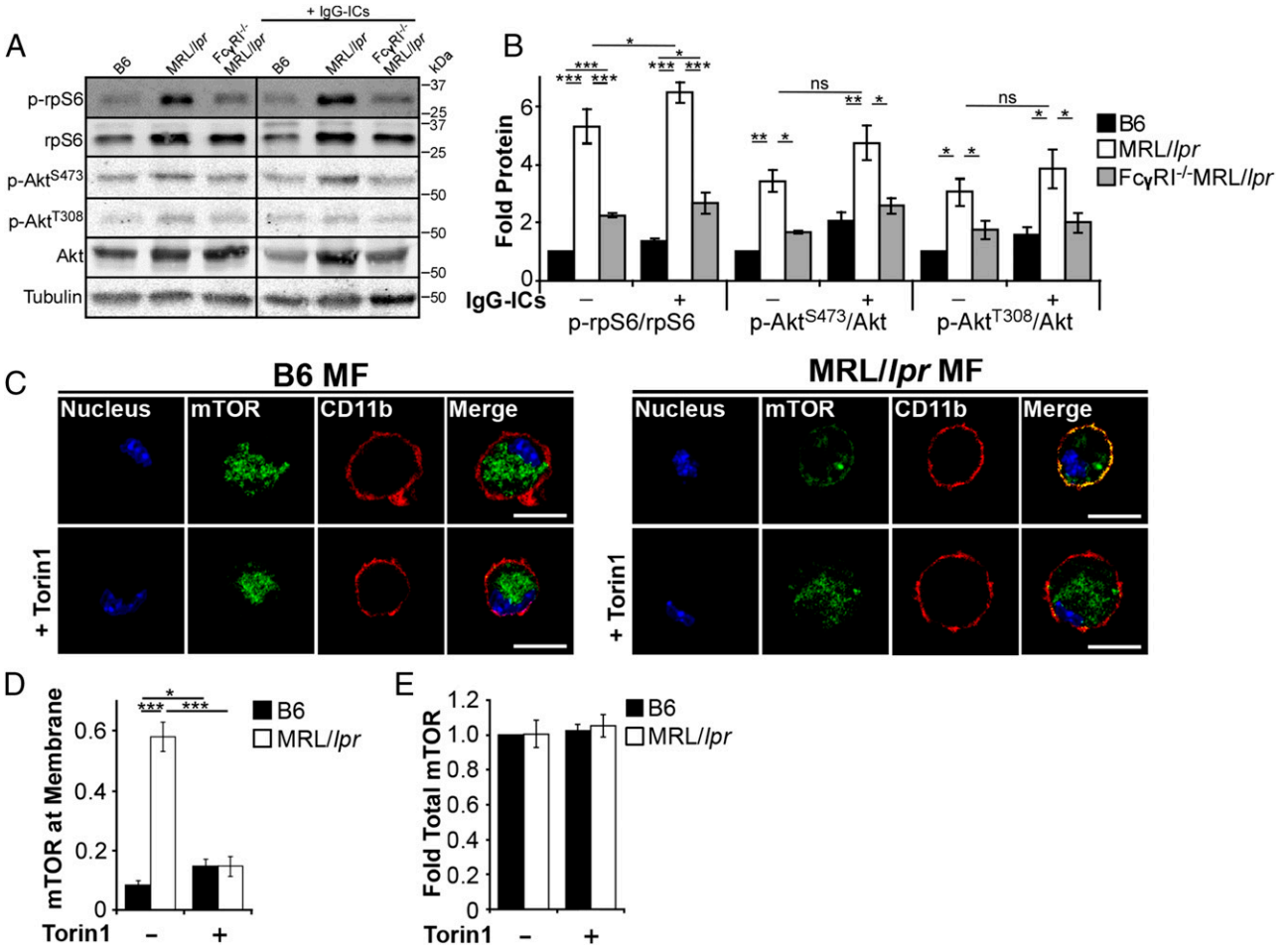

FIGURE 1. Lupus-prone Mφs have heightened and mislocalized mTOR activity. (**A** and **B**) Cell lysates from unstimulated and stimulated (1 h) BMMφs (1–1.5 × 10^6 cells) were immunoblotted with the indicated proteins; four experiments (exp) were conducted using four mice. Densitometry values were normalized to tubulin and relative to B6. (**C** and **D**) Unstimulated BMMφs treated ± Torin1 (250 nM) for 2 h were examined by confocal imaging for mTOR localization with CD11b (scale bar, 10 μm); three exp were conducted using three mice and 30 cells. (**E**) Unstimulated BMMφs were cultured ± Torin1 (250 nM) for 2 h, and the levels of mTOR were assessed by flow cytometry; three exp were conducted using three mice. The MFI was normalized to the isotype control and relative to untreated B6. Data are presented as mean ± SEM. *$p \leq 0.05$, **$p \leq 0.01$, ***$p \leq 0.001$.

IgG-IC. This is consistent with our previous study showing that <5% of internalized IgG-ICs enter autophagosomal structures (13).

To determine whether the role of mTORC2 in lysosome acidification is unique to phagocytosis, we assessed an alternative form of internalization called LAP (30). Upon phagocytosis of large cargo (e.g., intact apoptotic cells) LC3A stabilizes the phagosomal membrane to form a LAPosomal structure. To assess LAP, we measured the levels of LC3A in Mφs following exposure to intact WC-ICs. Phagocytosis of WC-ICs increased LC3A levels 3.5- to 3.1-fold in B6 and MRL/*lpr* Mφs, an effect not seen post-phagocytosis of IgG-ICs (Fig. 2C). In addition, intact apoptotic cells (no IgG) also increased LC3A (Supplemental Fig. 1H), indicating that LAP is not influenced by IgG and might occur because of cargo size. To assess whether MRL/*lpr* Mφs exhibit defective lysosome acidification following LAP and whether this process is similarly influenced by mTORC2, we monitored vesicular pH following phagocytosis of WC-ICs. Although WC-ICs required more time to induce acidification (Fig. 2D) compared with IgG-ICs (Fig. 2A), the magnitude of lysosome acidification was comparable. As with IgG-ICs, phagocytosis of WC-ICs failed to promote acidification in MRL/*lpr* Mφs, and diminished acidification following LAP was not due to decreased LC3A expression, as these levels were comparable in MRL/*lpr* and B6 Mφs (Fig. 2C). To determine whether mTORC2 plays a similar role during LAP, we treated MRL/*lpr* Mφs with Torin1 or rapamycin. Torin1 restored lysosome acidification in MRL/*lpr* Mφs to levels comparable to B6, whereas rapamycin had no effect (Fig. 2D). These data demonstrate that chronic mTORC2 activity impairs lysosome acidification, regardless of the means of internalization. Further, these data raise the possibility that lupus-related pathologies associated with impaired LAP (31) could result from impaired lysosome maturation (13–15).

Chronic mTORC2 activity phosphorylates and mislocalizes cofilin

mTORC2 regulates actin dynamics by activating Rho GTPases (28) that, in turn, stimulate Lim kinases (LIMKs). LIMKs phosphorylate cofilin, thereby preventing actin depolymerization (32). We reasoned that chronic mTORC2 activity might inhibit lysosome acidification through a cofilin-dependent mechanism. In unstimulated MRL/*lpr* Mφs, the basal levels of p-cofilin were 1.5-fold higher than B6 (Fig. 3A, Supplemental Fig. 2A). After stimulation with IgG-ICs, p-cofilin levels were 2.4-fold higher than B6, a result confirmed by immunoblot (Fig. 3B, 3C). Further, inhibiting LIMK (LIMKi 3) (32), or mTORC1/C2 (Torin1) in MRL/*lpr* Mφs, reduced p-cofilin to levels comparable to B6 (Fig. 3A). In contrast, rapamycin (mTORC1 inhibitor) had no effect. Thus, chronic mTORC2 activity heightens cofilin phosphorylation. Because actin affects cellular motility, and chronic mTORC2 activity

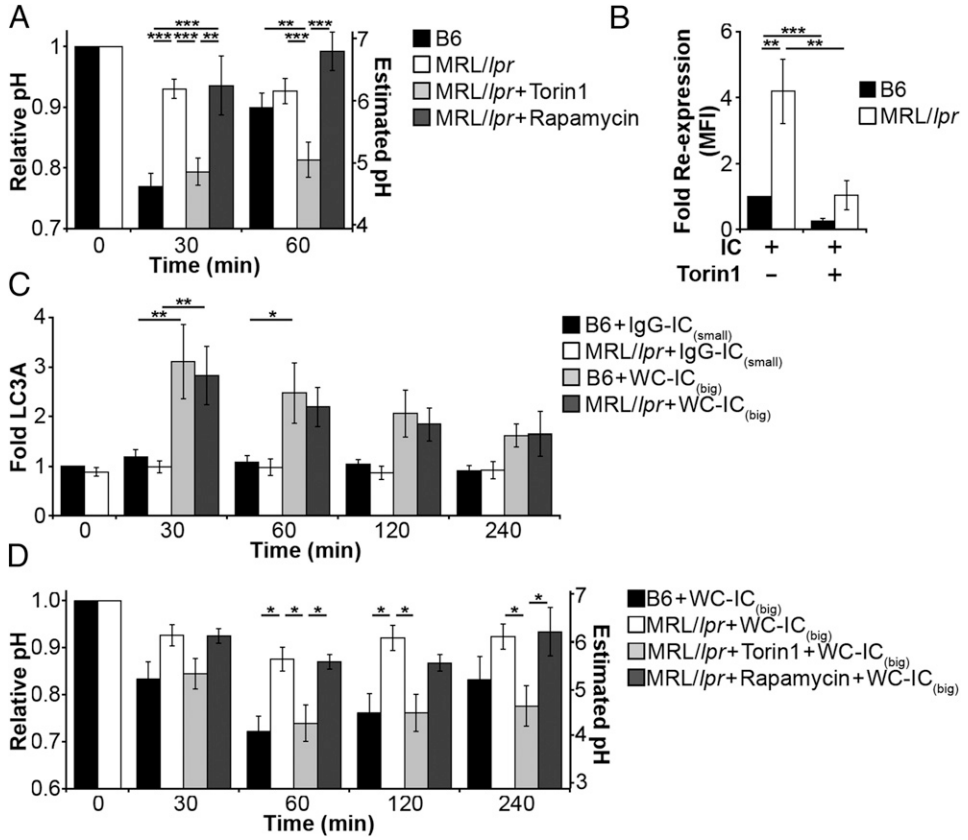

FIGURE 2. Chronic mTORC2 activity impairs lysosome acidification and degradation of IgG-ICs. BMMφs treated for 2 h ± Torin1 (250 nM) or ± rapamycin (100 ng/ml) were stimulated with IgG-ICs while remaining on treatment. (**A**) Lysosome pH was assessed by ratiometric flow cytometry at indicated time points; 13 experiments (exp) were conducted using 3–14 mice. (**B**) Recycling of surface IgG-ICs assessed by flow cytometry 72 h post-stimulation; five to six exp were conducted using five to six mice. (**C**) BMMφs were stimulated with IgG-ICs (small; representing apoptotic blebs bound by IgG) or WC-ICs (big; representing intact apoptotic cells bound by IgG), and LC3A levels were measured by flow cytometry; seven exp were conducted using seven mice. MFI was normalized to the isotype control and relative to unstimulated B6. (**D**) BMMφs treated for 2 h ± Torin1 (250 nM) or ± rapamycin (100 ng/ml) were stimulated with WC-ICs (big) while remaining on treatment. Lysosome pH was assessed by ratiometric flow cytometry at indicated time points; four exp were conducted using four mice. Data are presented as mean ± SEM. $*p \leq 0.05$, $**p \leq 0.01$, $***p \leq 0.001$.

prevents actin depolymerization (28), we predicted that MRL/*lpr* Mφs may exhibit decreased membrane ruffling and/or cell migration. Imaging of MRL/*lpr* Mφs showed that membrane ruffling (Supplemental Fig. 2B–D) and Mφ migration (Supplemental Fig. 2E–H) were decreased. This is consistent with previous findings that mobility of lupus-prone Mφs is decreased following exposure to lipids and/or apoptotic debris (33–35).

Cofilin attaches to F-actin and promotes depolymerization (36), whereas phosphorylation of cofilin prevents its association with actin, thereby stabilizing actin filaments (32). In MRL/*lpr* Mφs, active mTOR localizes to the cell membrane (Fig. 1C, 1D), coinciding with increased levels of p-cofilin (Fig. 3A). We reasoned that mTORC2 activity at the membrane could increase the local levels of p-cofilin, thereby decreasing the association of cofilin with actin that surrounds phagocytic vesicles. To assess this, we stimulated Mφs with IgG-ICs and found that 3.9-fold more cofilin localized to IgG-IC–containing vesicles in B6 Mφs compared with MRL/*lpr* (Fig. 3D, 3E). In addition, the cofilin that localized to IgG-IC–containing vesicles in B6 Mφs was rarely phosphorylated. Conversely, 2.7-fold more p-cofilin localized with IgG-IC–containing vesicles in MRL/*lpr* Mφs, indicating that cofilin phosphorylation occurs in proximity to the vesicle.

Our findings support a model where mTORC2-mediated phosphorylation of cofilin reduces its association with phagocytic vesicle. If the association of cofilin to vesicular actin was important in lysosome acidification, then preventing cofilin localization to actin filaments should inhibit lysosome acidification in B6 Mφs. JasP stabilizes actin by binding directly to F-actin, thereby preventing cofilin association (37). B6 Mφs treated with JasP showed diminished acidification, similar to MRL/*lpr*, suggesting an important role for cofilin localization with the phagosome in lysosome acidification (Fig. 3F). Conversely, we predicted that decreasing p-cofilin levels in MRL/*lpr* Mφs would restore cofilin localization and subsequent lysosome acidification. Indeed, treating MRL/*lpr* Mφs with LIMKi 3 restored lysosome acidification to levels comparable to B6 (Fig. 3F). These data implicate chronic mTORC2 activity in constitutively phosphorylating cofilin, which disrupts lysosome acidification.

Cofilin allows caspase-11 to associate with vesicles

Although caspases are strongly associated with cell death (38), they have alternative roles (9, 10, 39). For example, the CARD domain of caspase-11 associates with AIP-1 and cofilin and facilitates actin depolymerization (40). This raises the possibility that the association of caspase-11 with cofilin might be necessary for lysosome acidification. To test this, we immunoprecipitated caspase-11 and quantified the levels of associated cofilin. In unstimulated B6 and MRL/*lpr* Mφs, the levels of caspase-11 that bound to cofilin were comparable (Fig 4A, 4B). In contrast, stimulation with IgG-ICs induced 2.5-fold more caspase-11 to bind cofilin in B6 Mφs compared with MRL/*lpr*. This was not due to increased caspase-11 expression (Fig 4A, 4C). Interestingly, p-cofilin levels

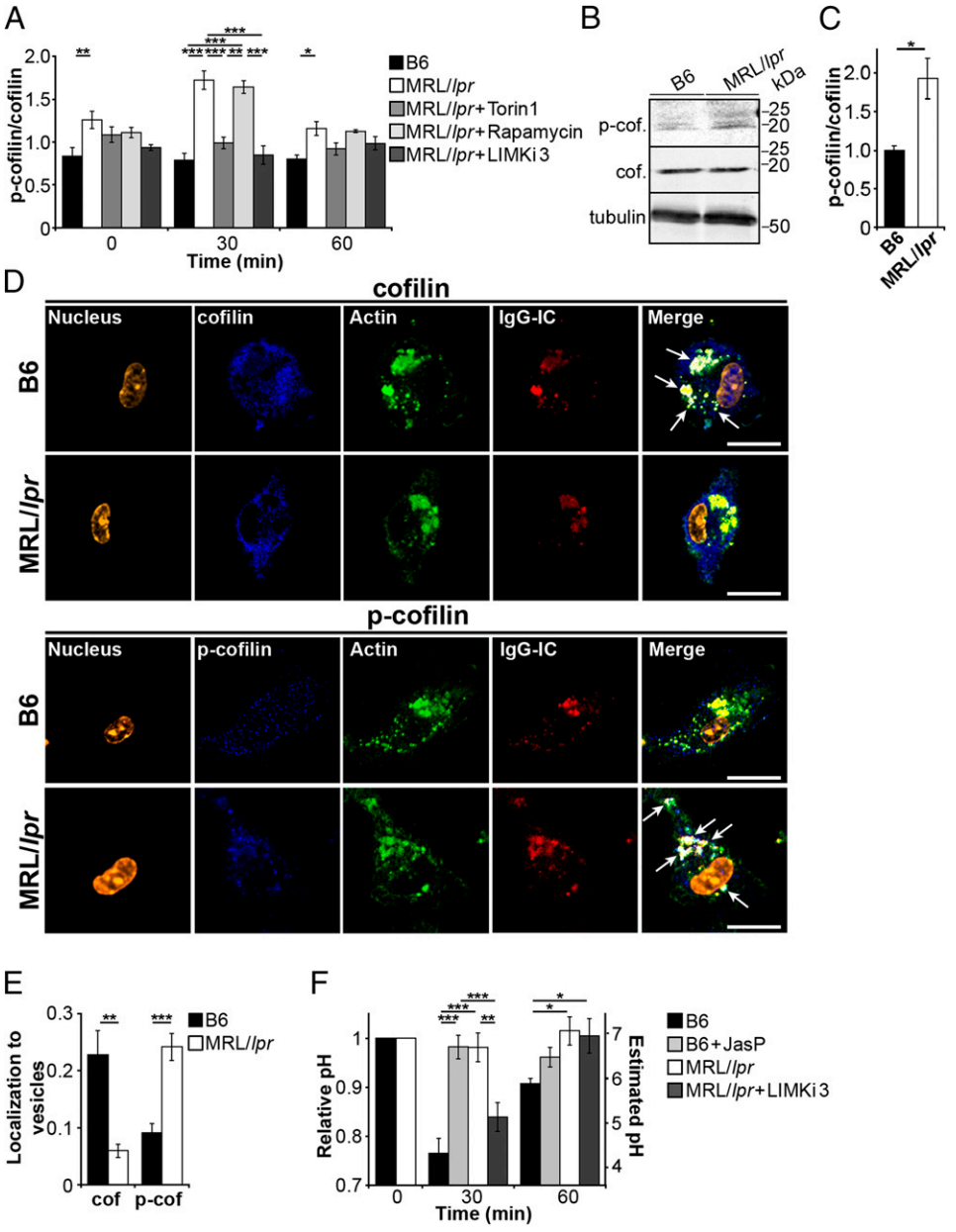

FIGURE 3. Chronic mTORC2 activity phosphorylates cofilin (cof), impairing lysosome acidification. (**A**) BMMφs treated for 2 h ± Torin1 (250 nM), ± rapamycin (100 ng/ml), or ± LIMKi 3 (3 μM) were stimulated with IgG-ICs while remaining on treatment. At the indicated time points, p-cofilin (p-cof) levels were measured by flow cytometry; ten experiments (exp) were conducted using three to ten mice. MFI was normalized to the isotype control, and p-cof was normalized to total cof. (**B** and **C**) Cell lysates from BMMφs (1–1.5 × 10^6 cells) stimulated with IgG-ICs (30 min) were measured by immunoblot; three exp were conducted using three mice. Densitometry values were normalized to tubulin and relative to B6. (**D** and **E**) BMMφs stimulated with IgG-ICs (15 min) were examined by confocal imaging in three dimensions for the localization of p-cof and cof with actin and IgG-ICs (scale bar, 5 μm); three exp were conducted using three mice and 13–14 cells. Colocalization was measured across the entire cell volume. (**F**) BMMφs treated for 1 h ± JasP (2 μM) or 2 h ± Torin1 (250 nM), ± rapamycin (100 ng/ml), or ± LIMKi 3 (3 μM) were stimulated with IgG-ICs while remaining on treatment. Lysosome pH was assessed by ratiometric flow cytometry at indicated time points; four exp were conducted using four mice. Data are presented as mean ± SEM. $^*p \leq 0.05$, $^{**}p \leq 0.01$, $^{***}p \leq 0.001$.

were undetectable, indicating that caspase-11 only associates with unphosphorylated cofilin (Fig. 4A). Thus, following phagocytosis of IgG-ICs, caspase-11 recruits to unphosphorylated cofilin.

Signaling effectors are normally recruited to phagosomal structures (11, 41). Therefore, proteins critical to lysosome acidification could also localize to vesicles containing IgG-ICs. Because cofilin associates with vesicles containing IgG-ICs (Fig. 3D, 3E), and caspase-11 is recruited to cofilin following stimulation with IgG-ICs (Fig. 4A–C), we hypothesized that caspase-11 could localize to vesicles containing IgG-IC. In B6 Mφs, we observed multiple instances of caspase-11 association with vesicles containing IgG-ICs, but in MRL/*lpr* Mφs, caspase-11 association was reduced 3-fold (Fig. 4D, 4E). This was not due to decreased caspase-11 expression (Fig. 4A, 4C). Further, caspase-11 retains its ability to associate with actin structures in MRL/*lpr* Mφs because we found significant colocalization of caspase-11 with actin that was not localized at vesicles containing IgG-ICs (Fig. 4D, 4E). This indicates that caspase-11 association with actin structures is not broadly impaired in MRL/*lpr* Mφs. In addition, impairing the phosphorylation of cofilin (LIMKi 3) and the activity of mTORC1/C2 (Torin1) in MRL/*lpr* Mφs restored the localization of caspase-11 to the vesicles containing IgG-ICs, whereas rapamycin had no effect (Fig. 4E, Supplemental Fig. 3A). This corroborates a role for chronic mTORC2 activity in preventing the association of caspase-11 with phagocytic vesicles when active LIMK phosphorylates cofilin.

Previous studies found that caspase-11 is important in lysosome acidification following phagocytosis of bacteria (9); however, the underlying mechanisms remain unclear. We found that caspase-11 recruits to vesicles containing IgG-ICs and that chronic mTORC2 activity in MRL/*lpr* Mφs prevents caspase-11 localization to the phagosome (Fig. 4D, 4E, Supplemental Fig. 3A). We reasoned that if caspase-11 were involved in lysosome acidification, BMMφs from B6.*caspase-11*$^{-/-}$ mice (Casp11$^{-/-}$) would show impaired acidification following phagocytosis of IgG-ICs. Lysosome acidification in Casp11$^{-/-}$ Mφs was impaired, with pH levels comparable to MRL/*lpr* (Fig. 4F). Together, these results demonstrate that localization of caspase-11 to phagocytic vesicles via cofilin is necessary to acidify the lysosome.

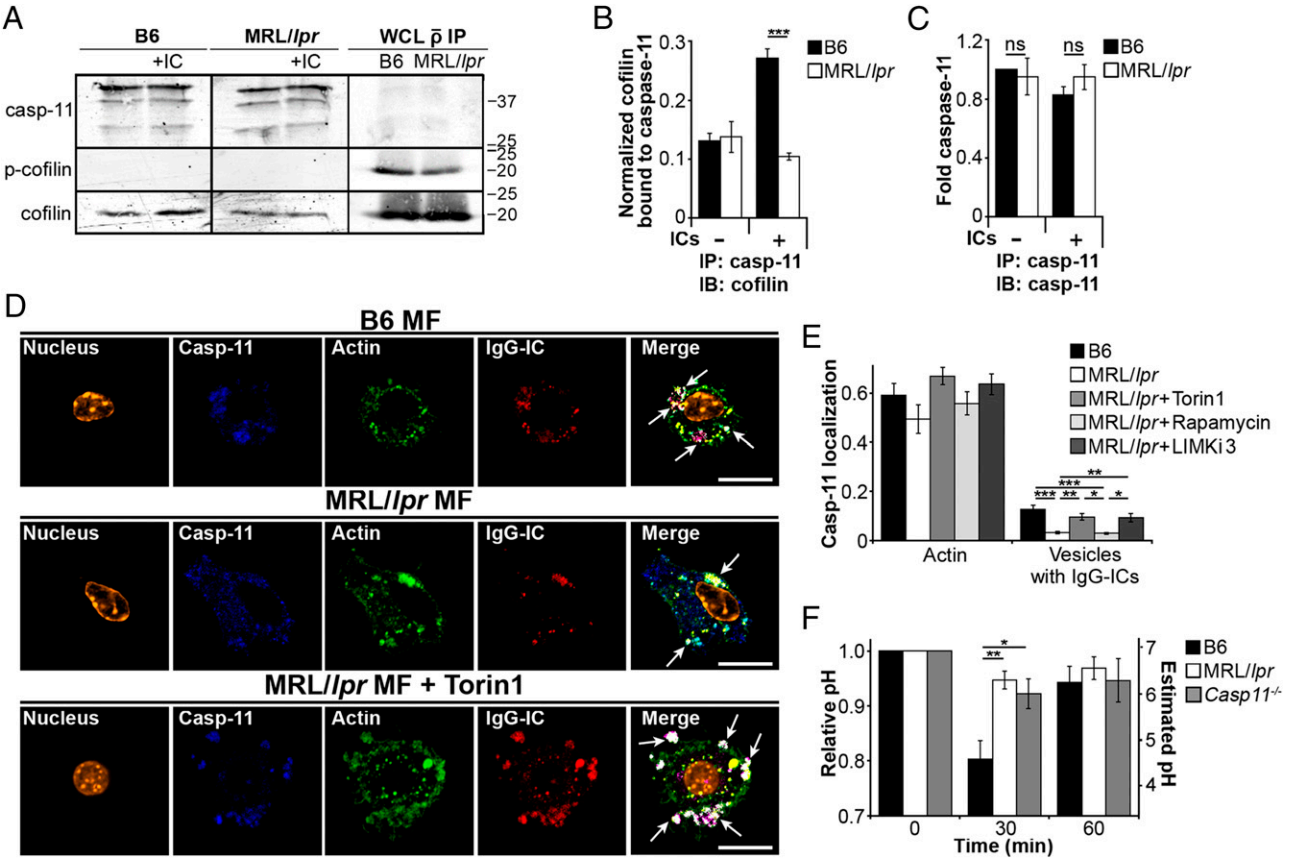

FIGURE 4. Phosphorylation of cofilin prevents caspase-11 localization with vesicles, which impairs lysosome acidification. (**A**–**C**) BMMφs were stimulated with IgG-ICs (30 min). Caspase-11 was immunoprecipitated (5–9 × 10^6 cells), and bound proteins were quantified by immunoblot; 5 experiments (exp) were conducted using three to five mice. Densitometry values were normalized to immunoprecipitated levels of caspase-11. (**D** and **E**) BMMφs treated for 2 h ± Torin1 (250 nM), ± rapamycin (100 ng/ml), or ± LIMKi 3 (3 μM) were stimulated for 15 min with IgG-ICs while remaining on treatment and were examined by confocal imaging in three dimensions for the localization of caspase-11 with actin and IgG-ICs (scale bar, 5 μm); three exp were conducted using three mice and 10–16 cells. Colocalization was measured across the entire cell volume. See Supplemental Fig. 3A for images of cells treated with LIMKi 3 and rapamycin. (**F**) BMMφs were stimulated with IgG-ICs, and lysosome pH was assessed by ratiometric flow cytometry at indicated time points; eight exp, five to eight mice. Data are presented as mean ± SEM. ns: $p > 0.05$, *$p \leq 0.05$, **$p \leq 0.01$, ***$p \leq 0.001$.

Caspase-11 recruitment to vesicles results in inflammasome-independent activation of caspase-1

Caspase-1 has been implicated in lysosome acidification after phagocytosis of bacteria, suggesting a role for caspase-1 beyond activation following inflammasome formation (10). Caspase-11 physically interacts with, and activates, caspase-1 (42). Therefore, the association of caspase-11 with phagocytic vesicles might locally activate caspase-1 upstream of lysosome acidification. Using immunoprecipitation, we assessed whether caspase-1 associates with caspase-11. Stimulation of B6 Mφs with IgG-ICs increased the association of caspase-1 with caspase-11 by 1.8-fold compared with MRL/*lpr* (Fig. 5A, 5B). This indicates that caspase-1 associates with caspase-11 in B6 Mφs following phagocytosis of IgG-ICs. In contrast, caspase-1 association with caspase-11 in MRL/*lpr* Mφs is impaired.

Stimulation of B6 Mφs recruits caspase-1 to caspase-11, coincident with a 2.1-fold increase in caspase-1 activity (Fig. 5C). In contrast, stimulation of MRL/*lpr* Mφs does not increase caspase-1 activity. To corroborate this result, we stimulated B6 and MRL/*lpr* Mφs with IgG-ICs, then immunoblotted lysates for the levels of caspase-1 p20 subunit (readout for caspase-1 activity). The p20 subunit was increased 4.3-fold in B6 Mφs compared with MRL/*lpr* (Fig. 5D, 5E). In addition, stimulation with IgG-ICs did not activate caspase-1 in BMMφs from Casp11$^{-/-}$ and B6.*caspase-1*$^{-/-}$*caspase-11*$^{-/-}$ mice (Casp1$^{-/-}$Casp11$^{-/-}$) (Fig. 5C). Thus, following phagocytosis, active caspase-1 associates with caspase-11 in B6 Mφs. However, association and activation are impaired in MRL/*lpr* Mφs.

Apoptosis-associated speck-like protein containing a caspase recruitment domain (ASC or Pycard) facilitates caspase-1 activation during inflammasome formation (18). To determine whether caspase-1 activation on the phagosome requires inflammasome formation, we measured the levels of active caspase-1 in BMMφs from B6.*pycard*$^{-/-}$ mice (Asc$^{-/-}$). Phagocytosis of IgG-ICs activated caspase-1 in Asc$^{-/-}$ Mφs to levels similar to B6 (Fig. 5C). This demonstrates that caspase-1 activation following phagocytosis is independent of ASC-mediated inflammasome formation but requires caspase-11. Consistent with activation of caspase-1 and caspase-11 being independent of pyroptosis, the activation of caspase-1 and recruitment of caspase-11 to the vesicles containing IgG-ICs did not result in cell death because B6 Mφs survived for over 72 h following phagocytosis (13).

Caspase-11 is integral to lysosome acidification (Fig. 4F) and necessary in activating caspase-1 following phagocytosis (Fig. 5C–E). Further, the correct localization of caspase-11 requires cofilin (Fig. 4E, Supplemental Fig. 3A). To assess whether these events were linked, we altered the function of cofilin and measured caspase-1 activation following stimulation of Mφs with IgG-IC. Impairing the association of cofilin with actin (JasP) reduced caspase-1 activation in B6 Mφs to levels comparable to MRL/*lpr* (Fig. 5F). Conversely, inhibiting cofilin phosphorylation (LIMKi 3)

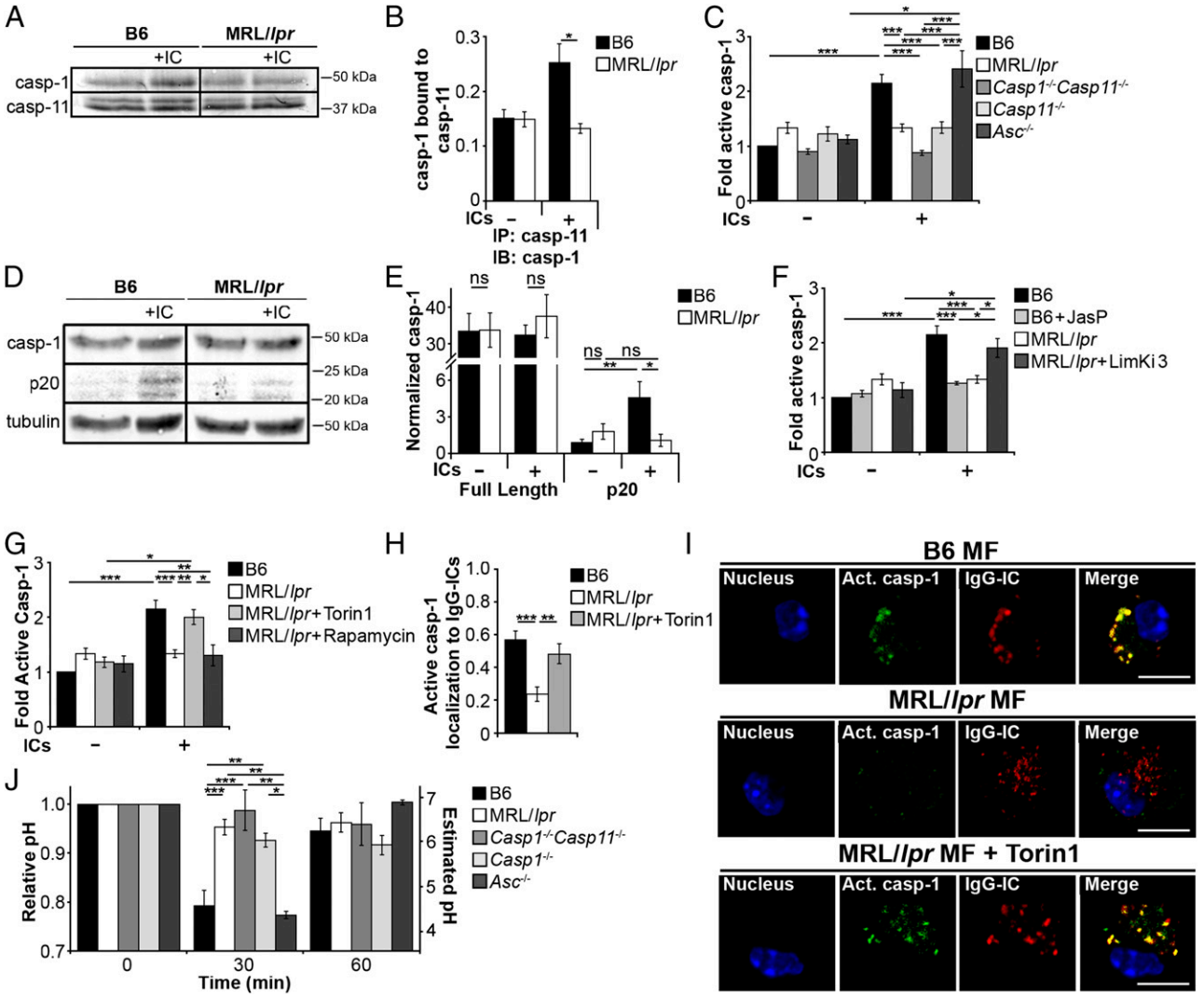

FIGURE 5. Mislocalization of caspase-11 prevents localized caspase-1 activation, thereby impairing lysosome acidification. (**A** and **B**) BMMφs were stimulated with IgG-ICs (30 min), and caspase-11 was immunoprecipitated (5–9 × 10^6 cells). Bound proteins were quantified by immunoblot; five experiments (exp) were conducted using five mice. Densitometry values were normalized to levels of immunoprecipitated caspase-11. (**C**) BMMφs were stimulated with IgG-ICs (30 min) and assessed for caspase-1 activation by flow cytometry; six exp were conducted using two to six mice. MFI of active caspase-1 is relative to unstimulated B6. (**D** and **E**) Cell lysates from BMMφs (4–4.5 × 10^6 cells) stimulated with IgG-ICs (30 min) were immunoblotted; four exp were conducted using four mice. Densitometry values were normalized to tubulin. (**F** and **G**) BMMφs treated for 1 h ± JasP (2 μM) or 2 h ± Torin1 (250 nM), ± rapamycin (100 ng/ml), or ± LIMKi 3 (3 μM) were stimulated with IgG-ICs (30 min) while remaining on treatment and assessed for caspase-1 activation by flow cytometry; six exp were conducted using two to six mice. MFI of active caspase-1 is relative to unstimulated B6. (**H** and **I**) BMMφs treated ± Torin1 for 2 h were stimulated with IgG-ICs (15 min) while remaining on treatment and were examined by confocal imaging to assess the localization of active caspase-1 with IgG-ICs (scale bar, 5 μm); three exp were conducted using three mice and 15–42 cells. (**J**) BMMφs stimulated with IgG-ICs and lysosome pH was assessed by ratiometric flow cytometry at indicated time points; nine exp were conducted using two to nine mice. Data are presented as mean ± SEM. ns: $p > 0.05$, *$p \leq 0.05$, **$p \leq 0.01$, ***$p \leq 0.001$. Casp-1, caspase-1.

restored caspase-1 activation in MRL/*lpr* Mφs to B6 levels. These results demonstrate that caspase-1 activation is dependent on the association of cofilin with actin.

Our data show that chronic mTORC2 activity and heightened phosphorylation of cofilin, mislocalize caspase-11 in MRL/*lpr* Mφs (Fig. 4E, Supplemental Fig. 3A). Further, phagocytosis in MRL/*lpr* Mφs did not localize caspase-1 to caspase-11 (Fig. 5A, 5B) or activate caspase-1 (Fig. 5C). Thus, it is possible that inhibiting mTORC2 might restore caspase-1 activation. Therefore, we treated MRL/*lpr* Mφs with Torin1 and stimulated them with IgG-ICs. Torin1 treatment increased caspase-1 activation 2-fold to levels seen in B6 Mφs (Fig. 5G). In contrast, treatment with rapamycin did not restore caspase-1 activity in MRL/*lpr* Mφs. This demonstrates that chronic mTORC2 activation limits caspase-1 activation following phagocytosis.

Because phagocytosis localizes caspase-11 to phagocytic vesicles (Fig. 4D, 4E) and activates caspase-1 (Fig. 5C–E), we reasoned that caspase-1 likely becomes activated in the proximity of vesicles containing IgG-ICs. Imaging showed that 3-fold more active caspase-1 localized with IgG-ICs in B6 Mφs compared with MRL/*lpr* (Fig. 5H, 5I). Torin1 treatment restored the localization of active caspase-1 with IgG-ICs in MRL/*lpr* Mφs to levels comparable to B6 (Fig. 5H, 5I). This is consistent with mTORC2 being upstream of caspase activation and reveals that phagocytosis initiates activation of caspase-1 proximal to phagocytic vesicles. Although 80–90% of MRL/*lpr* Mφs examined by microscopy showed low levels of caspase activation, there were rare cells that showed elevated levels of active caspase-1. In these instances, active caspase-1 was localized in the cytosol and did not colocalize with IgG-ICs. This staining pattern is consistent with

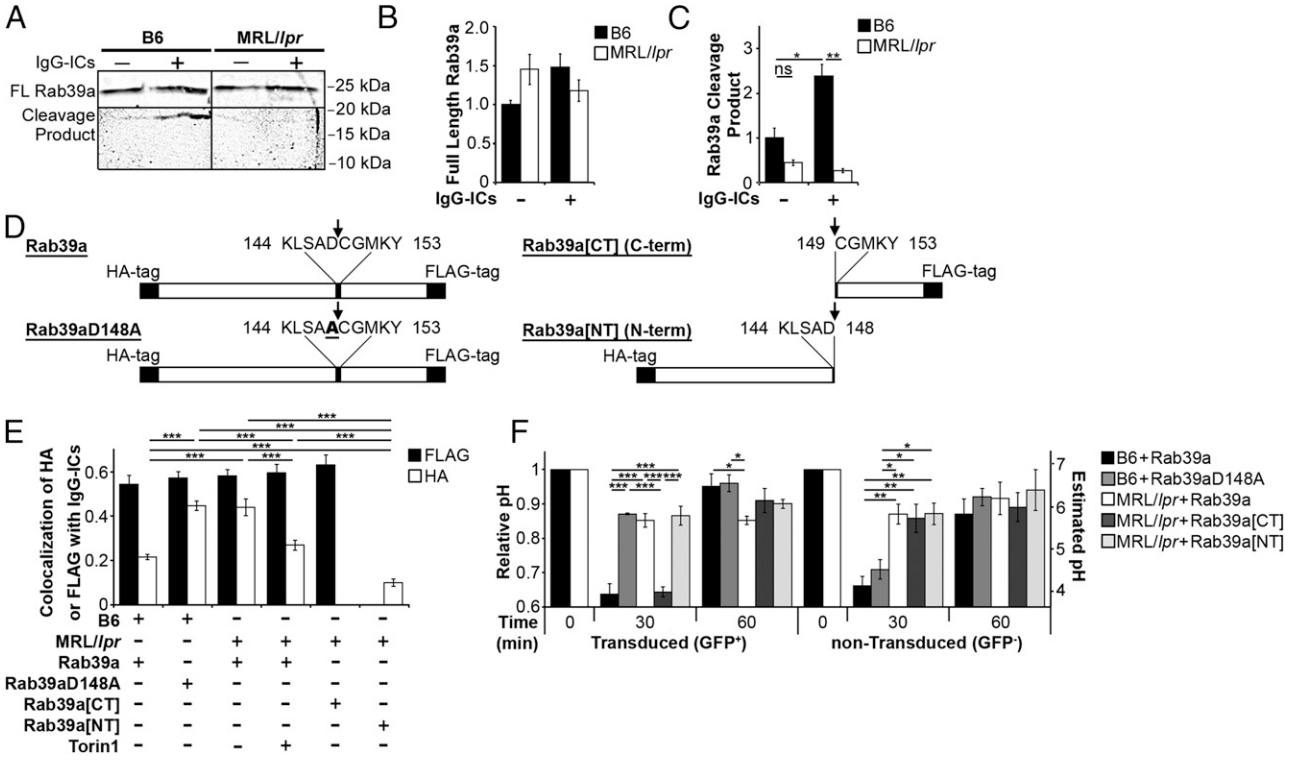

FIGURE 6. Failed cleavage of Rab39a by casapase-1 impairs lysosome acidification. (**A**–**C**) BMMφs were stimulated for 30 min with IgG-ICs, and Rab39a was immunoprecipitated (15–20 × 10^6 cells). Full-length (FL) Rab39a, or Rab39a cleavage product were quantified by immunoblot; three experiments (exp) were conducted using three mice. (**D**) Image showing the constructs used in retroviral transduction of BMMφs. Arrows point to caspase-1 cleavage site. (**E**) Transduced BMMφs treated for 2 h ± Torin1 (250 nM) were stimulated with IgG-ICs (20 min) while remaining on treatment. The confocal images showing the colocalization of Rab39a with IgG-ICs is quantified in (E), with representative images of the cells shown in Supplemental Fig. 4A; three exp were conducted using three mice and 16–21 cells. (**F**) Transduced BMMφs were stimulated with IgG-ICs. Lysosome pH was assessed in transduced (GFP^+) and nontransduced (GFP^-) Mφs over time using ratiometric flow cytometry; three exp were conducted using three mice. Data are presented as mean ± SEM. ns: $p > 0.05$, $*p \leq 0.05$, $**p \leq 0.01$, $***p \leq 0.001$.

inflammasome formation (Supplemental Fig. 3B) and supports our previous data, showing that impaired lysosome maturation in MRL/*lpr* Mφs allows nucleic acids from the IgG-ICs to leak into the cytosol and induce inflammasome formation (13).

To determine whether caspase-1 activation is necessary for lysosome acidification, we quantified the vesicular pH in BMMφs from B6.*caspase-1*$^{-/-}$*caspase-11*^{tg} (Casp1$^{-/-}$) mice after stimulation with IgG-ICs. Both Casp1$^{-/-}$Casp11$^{-/-}$ and Casp1$^{-/-}$ Mφs exhibited impaired lysosome acidification with pH levels comparable to MRL/*lpr* (Fig. 5J). Similarly, inhibiting caspase-1 with VAD-FMK prevented lysosome acidification in B6 Mφs (Supplemental Fig. 3C). The role of caspase-1 in lysosome acidification was inflammasome-independent, as Asc$^{-/-}$ Mφs achieve a pH comparable to B6 (Fig. 5J). It is important to note that Casp1$^{-/-}$ and Casp11$^{-/-}$ mice fail to develop spontaneous SLE despite having impaired lysosome acidification. Chronic mTORC1 activity in MRL/*lpr* Mφs (Fig. 1A, 1B) could impair autophagy. As such, Casp1$^{-/-}$ and Casp11$^{-/-}$ Mφs could use autophagic processes to degrade phagocytosed IgG-ICs when primary lysosome acidification fails (Supplemental Fig. 3D). Overall, this demonstrates that the localization of active caspase-1 with phagocytic vesicles is necessary to acidify the lysosome but is independent of inflammasomes.

Cleavage of Rab39a by caspase-1 is necessary for lysosome acidification

The association of Rab GTPases with specific membranes is critical for phagocytosis, vesicular trafficking, and exocytosis (1). Although the function of Rab39a is relatively uncharacterized, its subcellular localization suggests a role in endocytic pathways (43). Further, expression of a dominant-negative Rab39a prevents lysosome acidification (44), and Rab39a contains a functional caspase-1 cleavage site (45). Therefore, localization of active caspase-1 to phagocytic vesicles (Fig. 5H, 5I) could cleave Rab39a, leading to lysosome acidification. To assess this, we immunoprecipitated Rab39a and immunoblotted for full-length Rab39a and the 17-kDa N-terminal cleavage product. Following phagocytosis of IgG-ICs, B6 Mφs cleaved 9.6-fold more Rab39a compared with MRL/*lpr* Mφs (Fig. 6A–C).

Commercial Abs to Rab39a are limited, and they fail to spatially resolve Rab39a within the cell (data not shown). Therefore, we constructed FLAG- and HA-tagged versions of Rab39a (Fig. 6D), a Rab39a point mutant where Asp^{148} in the caspase-1 cleavage site was replaced by Ala (Rab39aD148A) to prevent caspase-1 cleavage (45) and the Rab39a[NT] and Rab39a[CT] caspase-1 cleavage products.

To define the role of Rab39a during vesicular trafficking, we transduced BMMφs with wild type and mutant forms of Rab39a and then used microscopy to monitor their localization relative to internalized IgG-ICs. In B6 BMMφs transduced with the uncleavable Rab39aD149A, both the HA and FLAG tags colocalized with IgG-ICs (Fig. 6E; representative images in Supplemental Fig 4A), consistent with the D149A mutation-impairing cleavage by caspase-1. In contrast, B6 BMMφs transduced with wild type Rab39a showed that the FLAG tag (C terminus) colocalized with IgG-ICs, whereas the HA tag (N terminus) showed a 2.1-fold reduction in colocalization with IgG-ICs. Therefore, Rab39a is cleaved in B6 Mφs with the C-terminal fragment remaining on

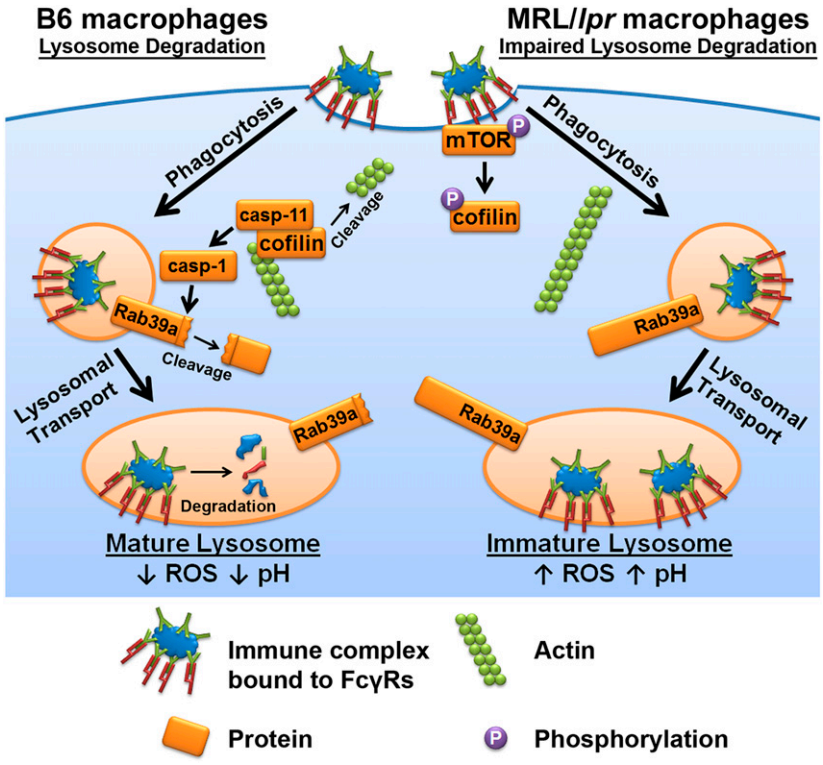

FIGURE 7. Model depicting the signaling events regulating lysosome acidification in B6 Mφs (left) and the signaling defects associated with impaired lysosome acidification in lupus-prone MRL/*lpr* Mφs (right).

the vesicle, and the N terminus dispersing into the cytosol. In MRL/*lpr* BMMφs expressing wild type Rab39a, a different phenotype was evident. We found that the HA (N terminus) and FLAG (C terminus) tags remained colocalized with IgG-ICs (Fig. 6E, Supplemental Fig. 4A). This was much like B6 Mφs expressing uncleavable Rab39aD148A, indicating that MRL/*lpr* Mφs fail to efficiently cleave Rab39a. To assess whether cleavage of Rab39a could be restored by inhibiting mTOR activity, we treated MRL/*lpr* Mφs with Torin1. Inhibiting mTOR reduced the colocalization of the HA tag (N terminus) with IgG-ICs by 1.6-fold (Fig. 6E, Supplemental Fig. 4A). This indicates that heightened mTOR activity disrupts the cleavage of Rab39a, coincident with diminished caspase-1 activation (Fig. 5G). To assess whether the N or C terminus of Rab39a is required for acidification, we transduced MRL/*lpr* Mφs with Rab39a[CT] or Rab39a[NT]. Cells expressing Rab39a[CT] showed the FLAG tag (C terminus) colocalized with IgG-ICs, whereas cells expressing Rab39a[NT] showed a 4.4-fold decrease in the colocalization of the HA tag (N terminus) with IgG-ICs when compared with MRL/*lpr* Mφs expressing wild type Rab39a (Fig. 6E). This corresponded with a diffuse cytosolic staining pattern (Supplemental Fig. 4A). The ability of the C terminus of Rab39a, but not the N terminus, to associate with the phagosomal membrane is consistent with previous studies showing that prenylation motif in the C terminus of Rab proteins is necessary for membrane association (46).

Although a dominant-negative form of Rab39a prevents lysosome acidification (44), and the caspase-1 cleavage site in Rab39a is functional in vivo (45), cleavage of Rab39a by caspase-1 has never been associated with lysosome acidification. Like nontransduced B6 Mφs, those expressing wild type Rab39a showed a 36% decrease in pH after IgG-IC stimulation (Fig. 6F, gating scheme in Supplemental Fig. 4B). In contrast, B6 Mφs expressing uncleavable Rab39aD148A showed a 13% decrease in pH. This indicates that caspase-1 cleavage of Rab39a is necessary for lysosome acidification.

To define which Rab39a fragment was associated with lysosome acidification, we measured the ability of MRL/*lpr* Mφs expressing either the N- or C-terminal Rab39a cleavage products to acidify. MRL/*lpr* Mφs expressing Rab39a[CT] showed a 36% decrease in pH upon IgG-IC stimulation, which is comparable to B6 (Fig. 6F). In contrast, neither full-length wild type Rab39a nor Rab39a[NT] rescued lysosome acidification, achieving a 13–14% decrease in pH. This indicates that the C-terminal fragment of Rab39a can rescue the lysosome defect in MRL/*lpr* Mφs and thus is sufficient to acidify the lysosome. The inability of MRL/*lpr* Mφs to activate caspase-1 in the proximity of phagocytic vesicles (Fig. 5H, 5I) impairs Rab39a cleavage, which is necessary for lysosome acidification [see model (Fig. 7)].

Discussion

This study defines a previously unappreciated role for actin-dependent caspase-1 activation in lysosome acidification. In wild type Mφs, binding of IgG-ICs to FcγRI transiently increases mTORC2 activity, allowing cofilin to associate with the actin that surrounds phagocytic vesicles (phagosomes) containing the internalized IgG-ICs (Fig. 7). Cofilin subsequently recruits caspase-11, which, in turn, activates caspase-1 in proximity of the phagosome. Activated caspase-1 cleaves Rab39a, allowing its C-terminal fragment to promote lysosome acidification. This process is impaired in Mφs from lupus-prone mice. MRL/*lpr* Mφs exhibit chronic mTORC2 activity as part of a feedforward loop in which diminished lysosome acidification and recycling of IgG-ICs bound by FcγRI leads to chronic FcγRI signal transduction (Fig. 1A, 1B; (13, 14). Heightened mTORC2 activity increases the phosphorylation of cofilin; a form of cofilin that fails to associate with or depolymerize actin (Fig. 7). This disrupts the localization of caspase-11 with actin and prevents activation of caspase-1 at the phagocytic vesicle. As a result, Rab39a remains intact and lysosome acidification is impaired. Thus, in lupus-prone Mφs, impaired lysosome acidification prevents the degradation of IgG-ICs through sustained FcγRI signal transduction, creating a feedforward loop that promotes lupus-associated pathologies (13–15).

Autophagy is an alternative form of lysosomal degradation that primarily degrades damaged organelles and cytosolic proteins.

When impaired lysosomal acidification diminishes degradation of cargo in phagosomes, it is possible that autophagy can compensate by degrading immature phagolysosomes. Although Mφs from Casp11$^{-/-}$ mice exhibited diminished lysosome acidification, they do not develop SLE. However, they expressed high levels of LC3A (Supplemental Fig. 3D) consistent with autophagosome formation. In contrast, LC3A was not elevated in MRL/*lpr* Mφs, indicating that lupus-prone Mφs do not use autophagy, despite loss of lysosomal degradation. This could be a consequence of heightened mTORC1 activity (Fig. 1A, 1B) because mTORC1 has been shown to inhibit the assembly of autophagosomes (29), and mTORC1 is heightened in MRL/*lpr* Mφs as a consequence of chronic FcγRI signal transduction (Fig. 1A, 1B).

Our finding that activated caspase-1 was required for lysosome acidification was unexpected. Caspase-1 activation has historically been associated with inflammasomes and pyroptosis (17). Our findings reveal that caspase-1 also plays a critical role in lysosome acidification. Although it remains possible that NLRC4 or NLRP1b (CARD-containing receptors that don't require ASC for cell death) contribute to caspase-1 activity (47, 48), this scenario is unlikely because CARD-containing receptors still require ASC for downstream signal transduction (49). We do not believe CARD-containing receptors activate caspase-1 during lysosome acidification because they initiate pyroptosis (47, 48), yet we find that B6 Mφs that phagocytosed IgG-ICs survive longer than 72 h (13). However, this raises the following question: Why does activation of caspase-1 during lysosome acidification not promote cell death? One possibility is that varying levels of active caspase-1 promote different outcomes. Perhaps low levels of active caspase-1 induce lysosome acidification, whereas high levels drive pyroptosis. In support of this graded response, other studies show that low levels of caspase-3 or -8 activation regulate autophagic cell death, differentiation and proliferation of T and B cells, and maturation of dendritic cells (39), whereas high levels of activation promote apoptosis (38). Alternatively, localizing activated caspase-1 to vesicles (Fig. 5H, 5I) might restrict its activity near Rab39a on vesicular membranes. The importance of caspase-1 localization to its function has already been demonstrated in the context of pyroptosis, as localizing gasdermin D near the developing inflammasome directs its cleavage by caspase-1 (50). Localizing caspase-1 to vesicular membranes to promote lysosome acidification could further benefit the cell by heightening its pyroptotic potential. This would allow cells to respond to pathogens that breach the phagosomal membrane prior to their degradation in the phagolysosome. Thus, any pathogens that escape the phagosome are rapidly detected using the same caspases that promote their degradation. An unfortunate consequence of this potential host survival mechanism could be that environmental and/or genetic defects disrupting lysosome maturation result in autoimmune diseases like SLE.

It is noteworthy that p-rpS6 and p-Akt levels were heightened in MRL/*lpr* BMMφs prior to IgG-ICs stimulation. This might be a consequence of C-reactive protein (CRP), a serum acute-phase protein that opsonizes apoptotic debris. CRP produced by BMMφs, and present in serum, opsonizes cell debris generated during in vitro culture (data not shown). It is possible this source of cell debris cross-links and activates FcγRI at a low level in the absence of IgG (51). Both IgG and CRP activate similar downstream signaling effectors (52), fail to be degraded (13), and accumulate on the surface of hematopoietic cells in SLE (14). Interestingly, IgG-ICs are pathogenic, whereas CRP-opsonized apoptotic debris is protective during autoimmune disease (53). This difference could reflect CRP coengaging undefined inhibitory receptors (54), preventing long-term cellular activation in vivo or IgG binding additional activating receptors, leading to heightened cellular activation (13). The mechanisms of how these two FcγRI ligands confer protection versus pathologic conditions remain to be elucidated. Regardless, FcγRI-mediated signal transduction links incoming cargo to lysosome acidification.

Collectively, our studies show that accumulation of nuclear Ags on the surface of hematopoietic cells in murine SLE occurs prior to the onset of disease, is not unique to MRL/*lpr* mice, is not a consequence of Fas, and is not simply due to an increased burden of apoptotic cells (14). Biologically, lysosome dysfunction impacts disease at several levels. First, studies in FcγRI$^{-/-}$MRL/*lpr* mice and passive transfer of pathogenic IgG antinucleosome into AID$^{-/-}$MRL/*lpr* mice show that lysosome dysfunction is upstream of BAFF and IFN-α secretion, B cell activation, autoantibody production, migration of cells to the kidney, and renal disease (14, 15). This suggests that lysosome dysfunction is a "branch-point" upstream of multiple SLE-related pathologies. Second, defective degradation of IgG-ICs prolongs the exposure of endosomal TLRs to their ligands that are exposed on apoptotic debris/blebs. Diminished degradation of internalized IgG-ICs also permeabilizes the phagolysosomal membrane, allowing intact IgG-ICs to leak into the cytosol and activate innate receptors, heightening cell death and producing IFN-α (13). This provides an explanation for how cytosolic innate immune sensors become activated and contribute to SLE. This study identifies a previously unappreciated signaling pathway that regulates lysosome acidification and shows how lysosome dysfunction is linked to chronic FcγRI signal transduction and subsequent mTORC2 activity. We show that chronic mTORC2 activity disrupts assembly of caspase-11/caspase-1/Rab39a, a critical enzyme complex involved in lysosome acidification that normally assembles on the actin surrounding the phagolysosome. When this pathway is disrupted, incoming IgG-ICs are unable to be degraded and subsequently recycle to the cell surface. This creates a feedforward loop wherein chronic FcγR signaling, through heightened mTORC2 activity and disrupted assembly of caspase11/caspase1/Rab39a, attenuates lysosomal acidification. Thus, diminished lysosomal acidification and recycling of FcγRI-bound IgG-ICs result from, and lead to, chronic FcγR signaling. It is noteworthy that sustained signal transduction through FcγRI also activates mTORC1 (Fig. 1A, 1B). This may prevent autophagy from compensating for diminished lysosome degradation (28) and further cripple the clearance of inflammatory IgG-ICs.

Acknowledgments

We thank Ed Miao, Manira Rayamajhi, Jenny Ting, June Brickey, Jim Bear, Jeremy Rotty, Tony Richardson, Lance Thurlow, Mark McCrory, and Alex Szalai for generous advice, assistance, and reagents. We also thank the Flow Cytometry Core and the Microscopy Services Laboratory at the University of North Carolina at Chapel Hill for their support.

Disclosures

The authors have no financial conflicts of interest.

References

1. Stenmark, H. 2009. Rab GTPases as coordinators of vesicle traffic. *Nat. Rev. Mol. Cell Biol.* 10: 513–525.
2. Raiborg, C., and H. Stenmark. 2009. The ESCRT machinery in endosomal sorting of ubiquitylated membrane proteins. *Nature* 458: 445–452.
3. Chen, J. W., T. L. Murphy, M. C. Willingham, I. Pastan, and J. T. August. 1985. Identification of two lysosomal membrane glycoproteins. *J. Cell Biol.* 101: 85–95.
4. Flannagan, R. S., G. Cosío, and S. Grinstein. 2009. Antimicrobial mechanisms of phagocytes and bacterial evasion strategies. *Nat. Rev. Microbiol.* 7: 355–366.
5. Slauch, J. M. 2011. How does the oxidative burst of macrophages kill bacteria? Still an open question. *Mol. Microbiol.* 80: 580–583.
6. Rybicka, J. M., D. R. Balce, M. F. Khan, R. M. Krohn, and R. M. Yates. 2010. NADPH oxidase activity controls phagosomal proteolysis in macrophages

through modulation of the lumenal redox environment of phagosomes. *Proc. Natl. Acad. Sci. USA* 107: 10496–10501.
7. Gomez, T. S., J. A. Gorman, A. A. de Narvajas, A. O. Koenig, and D. D. Billadeau. 2012. Trafficking defects in WASH-knockout fibroblasts originate from collapsed endosomal and lysosomal networks. *Mol. Biol. Cell* 23: 3215–3228.
8. Zheng, K., K. Kitazato, Y. Wang, and Z. He. 2016. Pathogenic microbes manipulate cofilin activity to subvert actin cytoskeleton. *Crit. Rev. Microbiol.* 42: 677–695.
9. Akhter, A., K. Caution, A. Abu Khweek, M. Tazi, B. A. Abdulrahman, D. H. Abdelaziz, O. H. Voss, A. I. Doseff, H. Hassan, A. K. Azad, et al. 2012. Caspase-11 promotes the fusion of phagosomes harboring pathogenic bacteria with lysosomes by modulating actin polymerization. *Immunity* 37: 35–47.
10. Sokolovska, A., C. E. Becker, W. K. Ip, V. A. Rathinam, M. Brudner, N. Paquette, A. Tanne, S. K. Vanaja, K. J. Moore, K. A. Fitzgerald, et al. 2013. Activation of caspase-1 by the NLRP3 inflammasome regulates the NADPH oxidase NOX2 to control phagosome function. *Nat. Immunol.* 14: 543–553.
11. Zoncu, R., L. Bar-Peled, A. Efeyan, S. Wang, Y. Sancak, and D. M. Sabatini. 2011. mTORC1 senses lysosomal amino acids through an inside-out mechanism that requires the vacuolar H(+)-ATPase. *Science* 334: 678–683.
12. Appelqvist, H., P. Wäster, K. Kågedal, and K. Öllinger. 2013. The lysosome: from waste bag to potential therapeutic target. *J. Mol. Cell Biol.* 5: 214–226.
13. Monteith, A. J., S. Kang, E. Scott, K. Hillman, Z. Rajfur, K. Jacobson, M. J. Costello, and B. J. Vilen. 2016. Defects in lysosomal maturation facilitate the activation of innate sensors in systemic lupus erythematosus. *Proc. Natl. Acad. Sci. USA* 113: E2142–E2151.
14. Kang, S., J. L. Rogers, A. J. Monteith, C. Jiang, J. Schmitz, S. H. Clarke, T. K. Tarrant, Y. K. Truong, M. Diaz, Y. Fedoriw, and B. J. Vilen. 2016. Apoptotic debris accumulates on hematopoietic cells and promotes disease in murine and human systemic lupus erythematosus. *J. Immunol.* 196: 4030–4039.
15. Kang, S., Y. Fedoriw, E. K. Brenneman, Y. K. Truong, K. Kikly, and B. J. Vilen. 2017. BAFF induces tertiary lymphoid structures and positions T cells within the glomeruli during lupus nephritis. *J. Immunol.* 198: 2602–2611.
16. Kayagaki, N., S. Warming, M. Lamkanfi, L. Vande Walle, S. Louie, J. Dong, K. Newton, Y. Qu, J. Liu, S. Heldens, et al. 2011. Non-canonical inflammasome activation targets caspase-11. *Nature* 479: 117–121.
17. Kuida, K., J. A. Lippke, G. Ku, M. W. Harding, D. J. Livingston, M. S. Su, and R. A. Flavell. 1995. Altered cytokine export and apoptosis in mice deficient in interleukin-1 beta converting enzyme. *Science* 267: 2000–2003.
18. Mariathasan, S., K. Newton, D. M. Monack, D. Vucic, D. M. French, W. P. Lee, M. Roose-Girma, S. Erickson, and V. M. Dixit. 2004. Differential activation of the inflammasome by caspase-1 adaptors ASC and Ipaf. *Nature* 430: 213–218.
19. Andrews, B. S., R. A. Eisenberg, A. N. Theofilopoulos, S. Izui, C. B. Wilson, P. J. McConahey, E. D. Murphy, J. B. Roths, and F. J. Dixon. 1978. Spontaneous murine lupus-like syndromes. Clinical and immunopathological manifestations in several strains. *J. Exp. Med.* 148: 1198–1215.
20. Sun, C., and R. Bernards. 2014. Feedback and redundancy in receptor tyrosine kinase signaling: relevance to cancer therapies. *Trends Biochem. Sci.* 39: 465–474.
21. Brown, E. J., P. A. Beal, C. T. Keith, J. Chen, T. B. Shin, and S. L. Schreiber. 1995. Control of p70 s6 kinase by kinase activity of FRAP in vivo. [Published erratum appears in 1995 *Nature* 378: 644.] *Nature* 377: 441–446.
22. Alessi, D. R., S. R. James, C. P. Downes, A. B. Holmes, P. R. Gaffney, C. B. Reese, and P. Cohen. 1997. Characterization of a 3-phosphoinositide-dependent protein kinase which phosphorylates and activates protein kinase Balpha. *Curr. Biol.* 7: 261–269.
23. Sarbassov, D. D., D. A. Guertin, S. M. Ali, and D. M. Sabatini. 2005. Phosphorylation and regulation of Akt/PKB by the rictor-mTOR complex. *Science* 307: 1098–1101.
24. Wang, L., I. Gout, and C. G. Proud. 2001. Cross-talk between the ERK and p70 S6 kinase (S6K) signaling pathways. MEK-dependent activation of S6K2 in cardiomyocytes. *J. Biol. Chem.* 276: 32670–32677.
25. Bridges, D., J. T. Ma, S. Park, K. Inoki, L. S. Weisman, and A. R. Saltiel. 2012. Phosphatidylinositol 3,5-bisphosphate plays a role in the activation and subcellular localization of mechanistic target of rapamycin 1. *Mol. Biol. Cell* 23: 2955–2962.
26. Gan, X., J. Wang, B. Su, and D. Wu. 2011. Evidence for direct activation of mTORC2 kinase activity by phosphatidylinositol 3,4,5-trisphosphate. *J. Biol. Chem.* 286: 10998–11002.
27. Thoreen, C. C., S. A. Kang, J. W. Chang, Q. Liu, J. Zhang, Y. Gao, L. J. Reichling, T. Sim, D. M. Sabatini, and N. S. Gray. 2009. An ATP-competitive mammalian target of rapamycin inhibitor reveals rapamycin-resistant functions of mTORC1. *J. Biol. Chem.* 284: 8023–8032.
28. Jacinto, E., R. Loewith, A. Schmidt, S. Lin, M. A. Rüegg, A. Hall, and M. N. Hall. 2004. Mammalian TOR complex 2 controls the actin cytoskeleton and is rapamycin insensitive. *Nat. Cell Biol.* 6: 1122–1128.
29. Noda, T., and Y. Ohsumi. 1998. Tor, a phosphatidylinositol kinase homologue, controls autophagy in yeast. *J. Biol. Chem.* 273: 3963–3966.
30. Martinez, J., R. K. Malireddi, Q. Lu, L. D. Cunha, S. Pelletier, S. Gingras, R. Orchard, J. L. Guan, H. Tan, J. Peng, et al. 2015. Molecular characterization of LC3-associated phagocytosis reveals distinct roles for Rubicon, NOX2 and autophagy proteins. *Nat. Cell Biol.* 17: 893–906.
31. Martinez, J., L. D. Cunha, S. Park, M. Yang, Q. Lu, R. Orchard, Q. Z. Li, M. Yan, L. Janke, C. Guy, et al. 2016. Noncanonical autophagy inhibits the autoinflammatory, lupus-like response to dying cells. [Published erratum appears in 2016 *Nature* 539: 124.] *Nature* 533: 115–119.
32. Ross-Macdonald, P., H. de Silva, Q. Guo, H. Xiao, C. Y. Hung, B. Penhallow, J. Markwalder, L. He, R. M. Attar, T. A. Lin, et al. 2008. Identification of a nonkinase target mediating cytotoxicity of novel kinase inhibitors. *Mol. Cancer Ther.* 7: 3490–3498.
33. Antoni, A., V. A. Patel, H. Fan, D. J. Lee, L. H. Graham, C. L. Rosch, D. S. Spiegel, J. Rauch, and J. S. Levine. 2011. Macrophages from lupus-prone MRL mice have a conditional signaling abnormality that leads to dysregulated expression of numerous genes. *Immunogenetics* 63: 291–308.
34. Fan, H., V. A. Patel, A. Longacre, and J. S. Levine. 2006. Abnormal regulation of the cytoskeletal regulator Rho typifies macrophages of the major murine models of spontaneous autoimmunity. *J. Leukoc. Biol.* 79: 155–165.
35. Longacre, A., J. S. Koh, K. K. Hsiao, H. Gilligan, H. Fan, V. A. Patel, and J. S. Levine. 2004. Macrophages from lupus-prone MRL mice are characterized by abnormalities in Rho activity, cytoskeletal organization, and adhesiveness to extracellular matrix proteins. *J. Leukoc. Biol.* 76: 971–984.
36. Arber, S., F. A. Barbayannis, H. Hanser, C. Schneider, C. A. Stanyon, O. Bernard, and P. Caroni. 1998. Regulation of actin dynamics through phosphorylation of cofilin by LIM-kinase. *Nature* 393: 805–809.
37. Bubb, M. R., A. M. Senderowicz, E. A. Sausville, K. L. Duncan, and E. D. Korn. 1994. Jasplakinolide, a cytotoxic natural product, induces actin polymerization and competitively inhibits the binding of phalloidin to F-actin. *J. Biol. Chem.* 269: 14869–14871.
38. Siegel, R. M. 2006. Caspases at the crossroads of immune-cell life and death. *Nat. Rev. Immunol.* 6: 308–317.
39. Shalini, S., L. Dorstyn, S. Dawar, and S. Kumar. 2015. Old, new and emerging functions of caspases. *Cell Death Differ.* 22: 526–539.
40. Li, J., W. M. Brieher, M. L. Scimone, S. J. Kang, H. Zhu, H. Yin, U. H. von Andrian, T. Mitchison, and J. Yuan. 2007. Caspase-11 regulates cell migration by promoting Aip1-Cofilin-mediated actin depolymerization. *Nat. Cell Biol.* 9: 276–286.
41. Marshall, J. G., J. W. Booth, V. Stambolic, T. Mak, T. Balla, A. D. Schreiber, T. Meyer, and S. Grinstein. 2001. Restricted accumulation of phosphatidylinositol 3-kinase products in a plasmalemmal subdomain during Fc gamma receptor-mediated phagocytosis. *J. Cell Biol.* 153: 1369–1380.
42. Wang, S., M. Miura, Y. K. Jung, H. Zhu, E. Li, and J. Yuan. 1998. Murine caspase-11, an ICE-interacting protease, is essential for the activation of ICE. *Cell* 92: 501–509.
43. Chen, T., Y. Han, M. Yang, W. Zhang, N. Li, T. Wan, J. Guo, and X. Cao. 2003. Rab39, a novel Golgi-associated Rab GTPase from human dendritic cells involved in cellular endocytosis. *Biochem. Biophys. Res. Commun.* 303: 1114–1120.
44. Seto, S., K. Tsujimura, and Y. Koide. 2011. Rab GTPases regulating phagosome maturation are differentially recruited to mycobacterial phagosomes. *Traffic* 12: 407–420.
45. Becker, C. E., E. M. Creagh, and L. A. O'Neill. 2009. Rab39a binds caspase-1 and is required for caspase-1-dependent interleukin-1beta secretion. [Published erratum appears in 2016 *J. Biol. Chem.* 291: 24800.] *J. Biol. Chem.* 284: 34531–34537.
46. Khosravi-Far, R., R. J. Lutz, A. D. Cox, L. Conroy, J. R. Bourne, M. Sinensky, W. E. Balch, J. E. Buss, and C. J. Der. 1991. Isoprenoid modification of rab proteins terminating in CC or CXC motifs. *Proc. Natl. Acad. Sci. USA* 88: 6264–6268.
47. Miao, E. A., I. A. Leaf, P. M. Treuting, D. P. Mao, M. Dors, A. Sarkar, S. E. Warren, M. D. Wewers, and A. Aderem. 2010. Caspase-1-induced pyroptosis is an innate immune effector mechanism against intracellular bacteria. *Nat. Immunol.* 11: 1136–1142.
48. Van Opdenbosch, N., P. Gurung, L. Vande Walle, A. Fossoul, T. D. Kanneganti, and M. Lamkanfi. 2014. Activation of the NLRP1b inflammasome independently of ASC-mediated caspase-1 autoproteolysis and speck formation. *Nat. Commun.* 5: 3209.
49. Dick, M. S., L. Sborgi, S. Rühl, S. Hiller, and P. Broz. 2016. ASC filament formation serves as a signal amplification mechanism for inflammasomes. *Nat. Commun.* 7: 11929.
50. Kayagaki, N., I. B. Stowe, B. L. Lee, K. O'Rourke, K. Anderson, S. Warming, T. Cuellar, B. Haley, M. Roose-Girma, Q. T. Phung, et al. 2015. Caspase-11 cleaves gasdermin D for non-canonical inflammasome signalling. *Nature* 526: 666–671.
51. Marnell, L., C. Mold, and T. W. Du Clos. 2005. C-reactive protein: ligands, receptors and role in inflammation. *Clin. Immunol.* 117: 104–111.
52. Chi, M., S. Tridandapani, W. Zhong, K. M. Coggeshall, and R. F. Mortensen. 2002. C-reactive protein induces signaling through Fc gamma RIIa on HL-60 granulocytes. *J. Immunol.* 168: 1413–1418.
53. Szalai, A. J., C. T. Weaver, M. A. McCrory, F. W. van Ginkel, R. M. Reiman, J. F. Kearney, T. N. Marion, and J. E. Volanakis. 2003. Delayed lupus onset in (NZB x NZW)F1 mice expressing a human C-reactive protein transgene. *Arthritis Rheum.* 48: 1602–1611.
54. Tebo, J. M., and R. F. Mortensen. 1990. Characterization and isolation of a C-reactive protein receptor from the human monocytic cell line U-937. *J. Immunol.* 144: 231–238.